

NGC 326: X-shaped no more

M.J. Hardcastle¹, J.H. Croston², T.W. Shimwell^{3,4}, C. Tasse^{5,6}, G. Gürkan⁷,
R. Morganti^{3,8}, M. Murgia⁹, H.J.A. Röttgering⁴, R.J. van Weeren⁴ and W.L. Williams⁴

¹ Centre for Astrophysics Research, School of Physics, Astronomy and Mathematics, University of Hertfordshire, College Lane, Hatfield AL10 9AB, UK

² Department of Physical Sciences, The Open University, Milton Keynes MK7 6AA, UK

³ ASTRON, Netherlands Institute for Radio Astronomy, Oude Hoogeveensedijk 4, Dwingeloo, 7991 PD, The Netherlands

⁴ Leiden Observatory, Leiden University, PO Box 9513, 2300 RA Leiden, The Netherlands

⁵ GEPI, Observatoire de Paris, CNRS, Université Paris Diderot, 5 place Jules Janssen, 92190 Meudon, France

⁶ Department of Physics & Electronics, Rhodes University, PO Box 94, Grahamstown, 6140, South Africa

⁷ CSIRO Astronomy and Space Science, PO Box 1130 & Bentley WA 6102, Perth, Australia

⁸ Kapteyn Astronomical Institute, University of Groningen, P.O. Box 800, 9700 AV Groningen, The Netherlands

⁹ INAF – Osservatorio Astronomico di Cagliari, Via della Scienza 5, I-09047 Selargius (CA), Italy

9 July 2019

ABSTRACT

We present new 144-MHz LOFAR observations of the prototypical ‘X-shaped’ radio galaxy NGC 326, which show that the formerly known wings of the radio lobes extend smoothly into a large-scale, complex radio structure. We argue that this structure is most likely the result of hydrodynamical effects in an ongoing group or cluster merger, for which pre-existing X-ray and optical data provide independent evidence. The large-scale radio structure is hard to explain purely in terms of jet reorientation due to the merger of binary black holes, a previously proposed explanation for the inner structure of NGC 326. For this reason, we suggest that the simplest model is one in which the merger-related hydrodynamical processes account for all the source structure, though we do not rule out the possibility that a black hole merger has occurred. Inference of the black hole-black hole merger rate from observations of X-shaped sources should be carried out with caution in the absence of deep, sensitive low-frequency observations. Some X-shaped sources may be signposts of cluster merger activity, and it would be useful to investigate the environments of these objects more generally.

Key words: galaxies: jets – galaxies: active – radio continuum: galaxies

1 INTRODUCTION

As every massive galaxy contains a supermassive black hole (BH: Magorrian et al. 1998), the formation of binary systems of black holes is widely believed to be the inevitable consequence of the observed major mergers between massive galaxies (Begelman et al. 1980). It remains unclear theoretically, as noted by Begelman et al., whether the binary pairs thus formed can merge on a timescale shorter than the Hubble time, though recent work suggests that this is indeed possible (e.g. Gualandris et al. 2017). Constraints on the supermassive BH merger rate are important not just because they constrain cosmological models of galaxy formation and evolution, but also because they provide predictions for the rates of BH-BH merging events (Wyithe & Loeb 2003) in future gravitational wave detectors such as pulsar timing arrays (Hobbs et al. 2010) or LISA (Amaro-Seoane et al. 2012).

Radio-loud active galaxies (RLAGN) – radio galaxies and radio-loud quasars – are important in studies of the supermassive BH merger rate because the synchrotron-emitting plasma deposited by their jets gives us a fossil record of the jet orientation over

timescales of the radio source lifetime (which may be hundreds of Myr or more). Assuming, as is widely accepted, that the axis of jet generation is determined by the black hole spin axis (Blandford & Znajek 1977), then the formation of a close binary BH of which one member is a RLAGN will lead first to signatures of jet precession (e.g. Krause et al. 2019) followed by, eventually, an abrupt re-orientation of the jet axis as the two BH merge into one. Of course, this scheme assumes that the conditions for jet generation (non-negligible rates of accretion of magnetized material) can persist during the close binary phase and be re-established after merger, which may not be the case. Nevertheless, it is important to search for examples of RLAGN that provide evidence for this merger process.

In an influential paper Merritt & Ekers (2002) argued that the X-shaped radio sources provide direct evidence for BH-BH mergers. These are RLAGN which show a pair of extended ‘wings’ at a large angle to the currently active pair of lobes. In the BH-BH merger model, the wings represent the former lobe direction before jet reorientation, while the current lobes tell us about the current jet axis. Hydrodynamical models, in which the wings are sim-

ply distorted backflow from the active lobes (Leahy & Williams 1984), have difficulties in explaining systems in which the wings are longer than the active lobes without appealing to a peculiar source environment, and so the merger explanation for the X-shaped source class is attractive, and has motivated a number of searches for evidence of BH-BH mergers or binary BH in these systems. Samples of candidate X-shaped galaxies have been generated by visual inspection of existing radio catalogues in order to carry out such searches (Cheung 2007; Cheung et al. 2009), and tests of expectations of the different models have been carried out, with some observations tending to favour unusual environments for X-shaped sources (Hodges-Kluck et al. 2010; Landt et al. 2010) while others have argued for a binary black-hole origin (Zhang et al. 2007).

The first winged source to be discovered (Ekers et al. 1978), and a prototype of the X-shaped class (Wirth et al. 1982), is the nearby radio galaxy B2 0055+26 or 4C 26.03, usually referred to by the name of its optical identification, NGC 326. In this paper we report on new observations of this galaxy with the Low-Frequency Array (LOFAR: van Haarlem et al. 2013) that show conclusively that the large-scale structure of the source is generated by hydrodynamical effects, presumably related to bulk motion with respect to the ambient medium. We argue that high-quality, sensitive observations are necessary before coming to the conclusion that any particular radio morphology is indicative of BH-BH merger.

Throughout the paper we use a cosmology in which $H_0 = 70$ km s⁻¹, $\Omega_m = 0.3$ and $\Omega_\Lambda = 0.7$. At the redshift of NGC 326 1 arcsec corresponds to 0.93 kpc. The spectral index α is defined in the sense $S \propto \nu^{-\alpha}$.

2 NGC 326

B2 0055+26 is a radio galaxy at a redshift of 0.0474 (Werner et al. 1999). Its total radio luminosity of 8×10^{24} W Hz⁻¹ at 1.4 GHz (Murgia et al. 2001) places it just below the nominal Fanaroff-Riley luminosity break (Fanaroff & Riley 1974) which tends to separate sources with and without compact hotspots, in contrast to other well-studied X-shaped sources which are generally FRII radio sources. The best radio images to date are those of Murgia et al. (2001), who observed it at several frequencies with the (pre-upgrade) NRAO Very Large Array (VLA), and their detailed total intensity and polarization maps are consistent with this picture; the source shows the centre-brightened, transverse-magnetic-field jets of an FRI source and little compact structure in the extended lobes.

The host galaxy, NGC 326 itself, is a dumb-bell galaxy with two optical nuclei (Wirth et al. 1982), with a projected separation of 6.6 kpc. Both nuclei are radio sources (Murgia et al. 2001) with the jets being associated with the northern one (Core 1 in the notation of Werner et al. 1999). The host galaxy is the brightest member of a small optical group, Zwicky 0056.9+2626 (Zwicky & Kowal 1968). Optical spectroscopy by Werner et al. (1999) measured a velocity dispersion of 599^{+230}_{-107} km s⁻¹, consistent with a poor cluster. In the X-ray, the environment was studied with the ROSAT PSPC by Worrall et al. (1995), who found asymmetrical diffuse X-ray emission with a temperature ~ 2 keV, consistent with the velocity dispersion in implying a poor cluster environment; the X-ray environment is bright enough, at the low redshift of the system, that the cluster is a member of the ROSAT Brightest Cluster Sample of Ebeling et al. (1998) under the name RXJ0058.9+2657. More recently Hodges-Kluck & Reynolds (2012) presented a Chandra observation which confirms the asymmetrical nature of the X-rays.

Table 1. Observations of NGC326 with LOFAR

Field ID	Observation date	Duration (h)	Target offset from pointing centre (deg.)
P013+26	2016-09-19	8	1.43
P013+26	2017-01-16	8	1.43
P016+26	2016-10-14	8	1.65
P014+29	2016-10-03	8	1.68

3 OBSERVATIONS

3.1 LOFAR

LOFAR has observed the NGC 326 field as part of the LOFAR Two-metre Sky Survey, LoTSS¹, a deep survey of the northern sky at 144 MHz (Shimwell et al. 2017). Four pointings were used to construct the image used in the current paper: observational details are listed in Table 1. The data were initially reduced with version 2.2 of the standard Surveys Key Science Project pipeline², as described by Shimwell et al. (2019). This pipeline carries out direction-dependent calibration using KILLMS (Tasse 2014; Smirnov & Tasse 2015) and imaging is done using DDFACET (Tasse et al. 2018). Version 2.2 of the pipeline makes use of enhancements to the calibration and imaging, particularly of extended sources, that were described briefly in section 5 of Shimwell et al. (2019) and will be discussed more fully by Tasse et al. (in prep.). Running this pipeline gives us a mosaiced image of the field around NGC326, in which the images made from the three separate pointings (P013+26 was observed twice in error) are combined in the image plane, with a resolution of 6 arcsec and an rms noise of 95 μ Jy beam⁻¹.

The surveys pipeline finds self-calibration solutions for large areas of sky, and is not expected necessarily to find the optimal solution for any given sky position. To enhance the quality of the images around NGC 326 further, we used the models derived from the pipeline to subtract off all modelled sources from all four fields, leaving only the data for NGC 326 and its immediate surroundings, averaged appropriately, and then carried out several iterations of phase and amplitude self-calibration on the combined dataset (after correction for the LOFAR station beam at the source position) in order to improve the accuracy of the calibration solutions at that location, using WSCLEAN (Offringa et al. 2014) as the imager. This process (which will be described in more detail by van Weeren et al. in prep.) gave us an image at the central frequency of 144 MHz with a resolution of 8.2×5.1 arcsec (beam position angle of 84° and an rms noise level around the radio source of 110μ Jy beam⁻¹). The image noise is slightly worse in this post-processed image, presumably as a result of residuals from the subtraction being averaged over the image, but the image fidelity should be better since the pointings are combined in the uv plane rather than the image plane and since we can derive accurate amplitude and phase solutions at the source position. We therefore adopt the post-processed image for our detailed study.

The LOFAR flux scale is known to be significantly uncertain due to difficulties in transferring calibration from a reference source to the target field, and the bootstrap process applied to the data (Hardcastle et al. 2016) does not necessarily completely counteract either this or self-calibration-induced flux-scale drift. The integrated 144-MHz flux density of NGC 326 (9.96 ± 0.01 Jy) compares well with the Culgoora 160-MHz flux density of 9.5 Jy (Slee

¹ <https://lofar-surveys.org/>

² <https://github.com/mhardcastle/ddf-pipeline>

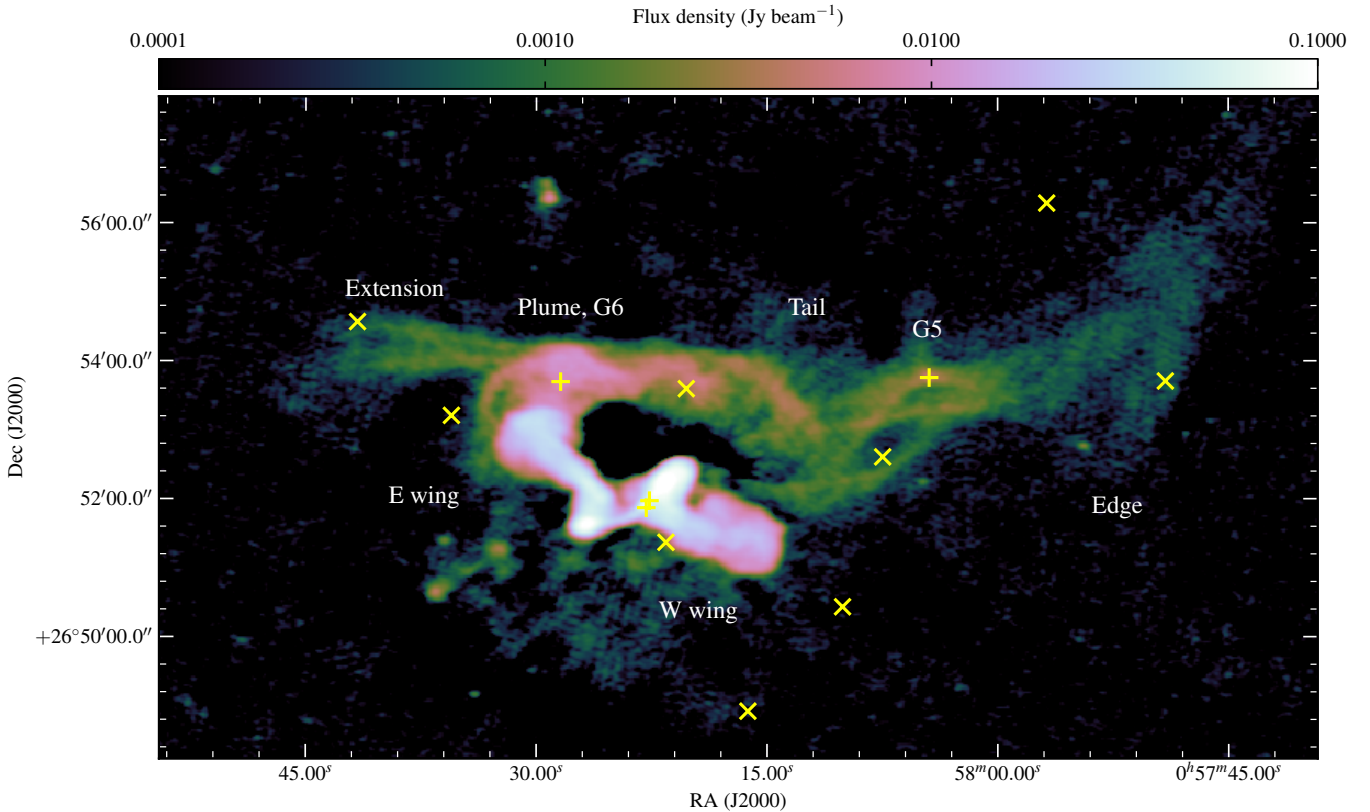


Figure 1. LOFAR colourscale of the radio emission from NGC 326. The colour scale is logarithmic over the range shown by the colour bar (in units of Jy beam^{-1} for the resolution of 8.2×5.1 arcsec), yellow crosses mark the positions of potential cluster members; + signs are those in the spectroscopic study of [Werner et al. \(1999\)](#) and × signs show candidate galaxies selected from NED as described in the text. The double nuclei of NGC 326 are represented by the two adjacent crosses close to the centre of the image. Features referred to in the text are labelled.

1995), given that the systematic errors on both flux densities are of order 10 per cent. The 4C flux density of 5.1 ± 0.6 Jy at 178 MHz ([Pilkington & Scott 1965](#)) will have been severely affected by resolution by the 4C interferometer and is not reliable. We were also able to check the flux scale with reference to the nearby bright (and relatively compact) source 3C 28, which has a measured 144-MHz flux density on the mosaiced pipeline output of 21.4 Jy, compared to an expectation from the measurements given by [Laing et al. \(1983\)](#) of 22.3 Jy (probably again with a ~ 10 per cent uncertainty). We conclude that the flux scale of the image is adequate for the purposes of this paper without further correction.

3.2 X-ray data

We downloaded the *Chandra* dataset, obsid 6830, described by [Hodges-Kluck & Reynolds \(2012\)](#) from the public archive and reprocessed it using CIAO 4.7 and the latest *Chandra* processing threads. In addition, we downloaded the *ROSAT* PSPC total-band image and exposure maps from the HEASARC archive and made a crude exposure-corrected image with 15-arcsec pixels, using the same data as described by [Worrall et al. \(1995\)](#), to illustrate the extent of the large-scale X-ray emission. As the focus of this work is the large-scale structure we have not applied any astrometric correction to the *ROSAT* data.

3.3 Optical data

For the purposes of probing the large-scale optical environment we supplemented the galaxies described by [Werner et al. \(1999\)](#) with other galaxies with spectroscopic redshifts taken from the Nasa Extragalactic Database (NED); principal redshift sources for NED include the Sloan Digital Sky Survey and the spectroscopic survey of [Cava et al. \(2009\)](#), who identified 22 cluster member candidates. Here we take as cluster member candidates any NED galaxy within 30 arcmin (1.7 Mpc) of NGC 326 having a velocity within 1500 km s^{-1} of the central velocity of $14,307 \text{ km s}^{-1}$ given by [Werner et al. \(1999\)](#) — the velocity range here is approximately 2.5 times the velocity dispersion of [Werner et al.](#). This gives a sample of 32 galaxies (including both nuclei of NGC 326) with a mean velocity of $14,530 \text{ km s}^{-1}$ and a velocity dispersion of 630 km s^{-1} , consistent with the measurements of [Werner et al.](#). The list of cluster member candidates is given in Table 2.

4 IMAGES

Fig. 1 shows the LOFAR image of NGC 326 as a colourscale. This image has several interesting features. The X-shaped structure seen in all previous observations is clearly visible in the centre of the image and is structurally very similar to what was seen in the images of [Murgia et al. \(2001\)](#). However, the east wing of the source has a clear and relatively bright extension, albeit with a drop of a factor ~ 3 in surface brightness, which continues northwards (the ‘plume’

Table 2. Galaxies selected from NED within 30 arcmin of NGC 326 and close in velocity space as described in the text. Data taken from NED.

Source name	RA	Dec	Heliocentric velocity (km s ⁻¹)	2MASS K_s	Werner name
NGC 0326 1	00h58m22.6s	+26d51m58.5s	14610 ± 15	11.822	G1-1
NGC 0326 2	00h58m22.8s	+26d51m52.4s	14822 ± 25	11.971	G1-2
2MASS J00582156+2651219	00h58m21.6s	+26d51m22.3s	13996 ± 7	13.658	
2MASS J00582023+2653357	00h58m20.2s	+26d53m35.9s	13809 ± 27	14.820	
2MASX J00582840+2653420	00h58m28.4s	+26d53m42.0s	15589 ± 30	12.742	G6
2MASX J00583550+2653121	00h58m35.5s	+26d53m12.6s	15600 ± 5	13.957	
2MASS J00581008+2650251	00h58m10.1s	+26d50m26.2s	14329 ± 31	14.940	
2MASS J00581623+2648549	00h58m16.2s	+26d48m55.4s	13737 ± 17	15.383	
GALEXASC J005807.41+265235.5	00h58m07.5s	+26d52m36.6s	14351 ± 87	No 2MASS	
MCG +04-03-024	00h58m04.5s	+26d53m45.6s	13850 ± 60	13.539	G5
2MASX J00580956+2647596	00h58m09.6s	+26d47m59.6s	14000 ± 30	12.680	G8
WINGS J005841.63+265434.1	00h58m41.6s	+26d54m34.1s	15795 ± 88	No photometry	
2MASX J00580702+2647545	00h58m07.0s	+26d47m55.5s	14776 ± 22	13.960	
2MASS J00575680+2656170	00h57m56.8s	+26d56m17.3s	15753 ± 19	14.691	
2MASS J00574910+2653421	00h57m49.1s	+26d53m42.5s	13593 ± 130	> 14.939	
WINGS J005812.33+264355.7	00h58m12.3s	+26d43m55.7s	14497 ± 57	No photometry	
2MASS J00584743+2658393	00h58m47.4s	+26d58m39.3s	13519 ± 19	12.277	G4
2MASX J00591642+2652009	00h59m16.4s	+26d52m01.7s	14856 ± 25	12.880	
2MASS J00591141+2658121	00h59m11.4s	+26d58m12.4s	14517 ± 99	No 2MASS	
2MASX J00572524+2650103	00h57m25.3s	+26d50m10.3s	14901 ± 14	12.846	
MCG +04-03-030	00h59m03.6s	+27d02m32.8s	14570 ± 30	12.260	G3
2MASS J00592575+2647599	00h59m25.8s	+26d48m00.7s	14841 ± 43	13.428	
2MASX J00592914+2655299	00h59m29.2s	+26d55m30.1s	14833 ± 43	13.727	
2MASX J00593281+2649476	00h59m32.8s	+26d49m48.0s	13875 ± 34	14.320	
2MASX J00591793+2704069	00h59m17.9s	+27d04m06.7s	15518 ± 75	13.456	
2MASX J00585376+2708030	00h58m53.8s	+27d08m03.7s	14901 ± 25	13.327	
UGC 613	00h59m24.4s	+27d03m32.6s	13770 ± 23	11.894	G2
2MASX J00590040+2708469	00h59m00.4s	+27d08m46.8s	14390 ± 30	12.139	G7
2MASXi J0059248+270720	00h59m24.8s	+27d07m21.0s	14386 ± 66	14.466	
2MASX J00594231+2639026	00h59m42.3s	+26d39m02.8s	14145 ± 45	13.681	
UGC 585	00h56m45.4s	+27d00m34.8s	13938 ± 22	12.075	
CGCG 480-031	01h00m27.9s	+27d01m30.8s	14914 ± 16	13.470	

just visible in the images of [Murgia et al.](#)) before bending sharply westward into a filamentary ‘tail’ structure that extends a total of 13 arcmin (720 kpc in projection) in an east-west direction. This feature, because of its angular size, would have been largely invisible to the VLA C-configuration L-band observations of [Murgia et al.](#) which were only sensitive to structures of scale < 6 arcmin. If they had had the required short baselines, the surface brightness of 4 mJy beam⁻¹ at 144 MHz in the bright parts of the tail should have been detectable to them at their observing frequency for $\alpha \sim 1$. No sensitive VLA D-configuration L-band observations of the target exist and so we cannot determine the LOFAR to VLA spectral index. Parts of the tail are plausibly detected at low significance in the NVSS survey, with the benefit of the LOFAR images to guide the eye, but are not well enough resolved from the wings and lobes or of sufficient signal to noise to allow a spectral index measurement. The integrated flux measurements of [Slee \(1995\)](#) imply $\alpha \approx 1.0$ for the whole source between 80 and 160 MHz and so it is plausible that the ‘tails’ are steep-spectrum.

A few other features of the tail structure are noteworthy. The connection between the west wing of the source and the tail is not as obvious as for the east wing, but several filamentary structures extend from the west wing towards the tail and may merge with it. One possibility is that there would be a high-surface-brightness extension of the west wing that is bent back behind the wing itself at our viewing angle; the wings may be much longer in projection than they are on the sky. In any case it seems likely that the tail structure is composed of plasma that originated in both lobes/wings

of the radio source; whether these are merged or just superposed in projection is not clear.

The filamentary structures in the tail are very striking. They cannot be imaging/deconvolution artefacts, since they appear essentially identical in our two high-resolution images made using WSCLEAN and DDFACET. We believe they provide evidence for large-scale coherent magnetic field enhancements: since we expect that the particles dominate the energy density in the tails ([Crosston et al. 2018](#)), field enhancements can exist and persist without creating a significant pressure difference within the tails. Similar filamentary structures exist in LOFAR observations of other tailed sources (e.g. 3C 83.1B, Bempong-Manful et al in prep.) – the excellent uv plane coverage of full-synthesis LOFAR observations makes them particularly sensitive to such structures. There is no immediately obvious explanation for the filamentary extension of the tail to the E of where it is entered by the plume of the E tail, or for its relatively sharp edge at the W end (see labels in Fig. 1 for the locations of these features).

Finally, we notice the remarkable alignment of 7 cluster candidate galaxies in an E-W direction on or close to the tail. The galaxy 2MASX J00582840+2653420 (G6 in the notation of [Werner et al. 1999](#)), which as noted by [Murgia et al. \(2001\)](#) is superposed on the ‘plume’, is not associated with any radio structure in the image; nor are any of the others, with the exception of MCG +04-03-024 (Werner’s G5, 2MASX J00580439+2653455), which lies directly on top of one of the bright filaments in the tail and has a compact radio counterpart. This galaxy is a disk system in the POSS-II images supplied by NED and has a bright X-ray counterpart in the

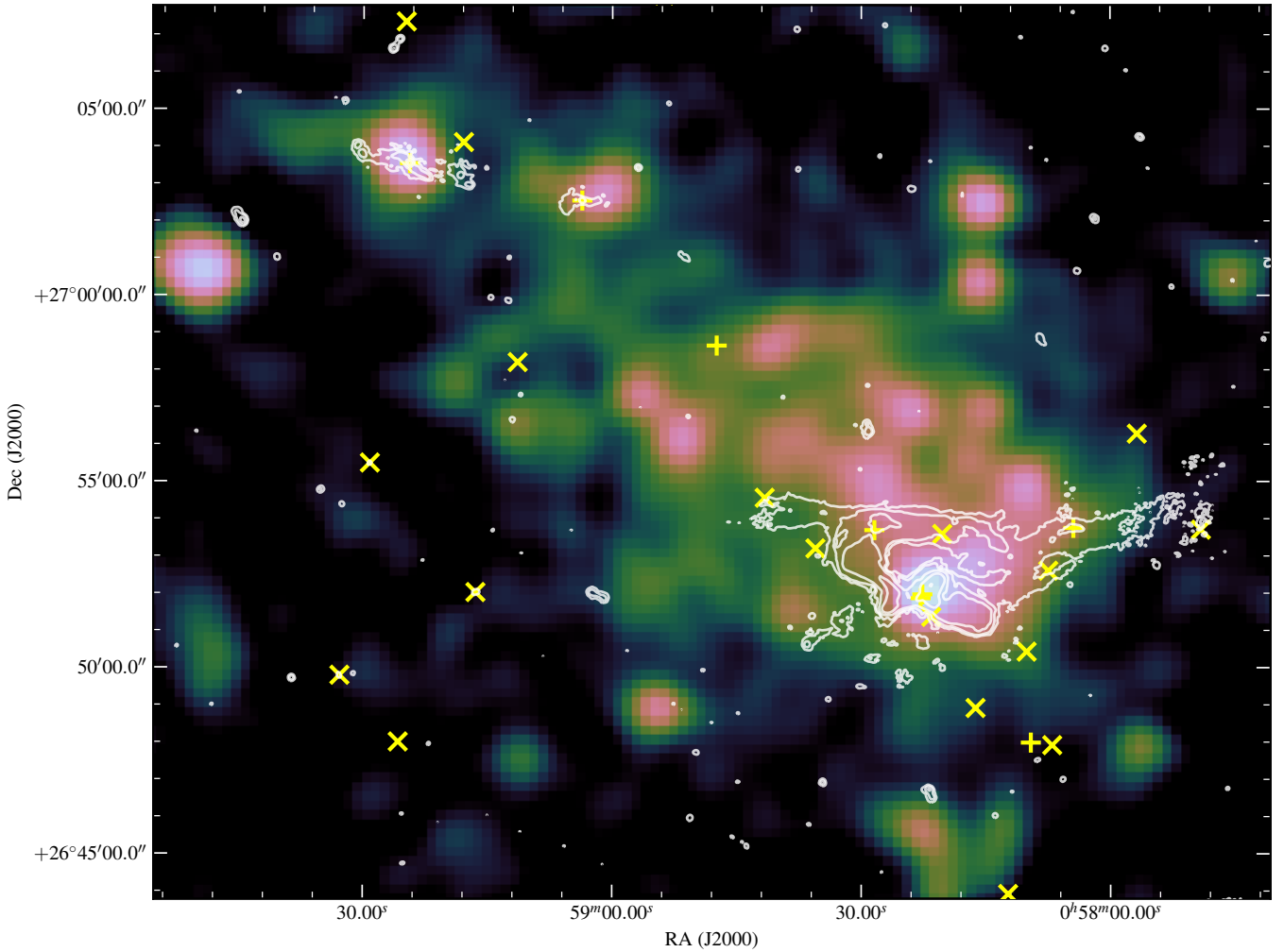


Figure 2. LOFAR contours of radio emission from the NGC 326 field (white, at $0.5 \times (1, 4, 16 \dots)$ mJy beam $^{-1}$) overlaid on a Gaussian-smoothed exposure-corrected *ROSAT* image with a logarithmic transfer function (colour). Crosses as in Fig. 1.

Chandra data, probably making it a Seyfert galaxy; it does not seem likely to us that it is directly responsible for any of the large-scale emission, including the filament it lies on, but clearly we cannot rule this out.

Fig. 2 shows the LOFAR image overlaid on the *ROSAT* data originally presented by Worrall et al. (1995). As they noted, the X-ray emission shows a strong elongation in a NE-SW direction, with NGC 326 lying to the SW. Another galaxy in the group, UGC 613 (G2 of Werner et al. 1999) is seen in the LOFAR images to be an extended radio source, with a flux density of around 300 mJy at 144 MHz, and has a compact *ROSAT* counterpart. A fainter extended radio source is associated with the neighbouring galaxy MCG +04-03-030, and this also has a much weaker X-ray counterpart seen in the *ROSAT* and *Chandra* data. Other radio sources in the field appear to be unrelated to the group. The X-ray properties of the group, together with the roughly bimodal distribution of member galaxies on the sky (one sub-group concentrated around NGC 326 and one more north-south extended group with UGC 613 as its most prominent member) are strongly suggestive of an unrelated, merging system. There is no clear relationship between the E-W direction of the radio tail and the NE-SW extension of the X-rays, either in the *ROSAT* or the higher-resolution *Chandra* data.

5 DISCUSSION AND CONCLUSIONS

The most obvious conclusion to be drawn from the deep LOFAR image is that NGC 326 can no longer be viewed as an archetype of the model in which jets are suddenly reoriented by BH-BH merger. The argument in favour of BH-BH merger for this source (Merritt & Ekers 2002) was based on the idea that hydrodynamical explanations for the lobe-wing structure, requiring complex hydrodynamic structure in the intra-cluster medium, were intrinsically less plausible than BH-BH mergers, which must after all occur. However, the extension of the wings into the large-scale tail structure *requires* a hydrodynamical explanation that can give rise to apparent sharp bends in the radio structure, and so in turn disfavors (on the principle of seeking the simplest possible explanation for the phenomena) any other explanation for the generation of the wings themselves. We emphasise that a BH-BH merger, either manifesting as an abrupt jet reorientation or as a slower transition mediated by gas associated with the merger as proposed by Zier (2005), is not ruled out by these data, but it is no longer either a necessary or a sufficient explanation for the observed source morphology on its own. Worrall et al. (1995), who favoured buoyancy as the bending mechanism for the wings, suggested that the extension of the E wing that was just visible in their data might be due to the plasma from the

wing reaching neutral buoyancy (i.e. the point where the density of the radio structure matches that of its surroundings), but it is difficult to see that on its own this model can account for the scale of the tail structure that we now see, with an elongation several hundred kpc away from the injection point through what are presumably very different conditions in the intracluster medium. While buoyancy must necessarily play a role, we suggest that complex large-scale bulk motions within the X-ray-emitting medium induced by the ongoing cluster merger, coupled with motions of the host galaxy itself with respect to that medium, are the only viable explanation for the observed radio structure in NGC 326. The same complex cluster hydrodynamics which account for the tail can plausibly then also account for the bending of the (no doubt projected) inner lobes into the wings. Such explanations still face difficulties; the 700-kpc projected length of the tail, if generated in a plausible AGN lifetime of 10^8 years, requires bulk growth speeds around 7000 km s^{-1} , much higher than the velocity dispersion or sound speed of the cluster, and so either high bulk speeds or a much larger source age are required. The significant change in surface brightness of the radio structures between the wings and the tail may also suggest some intermittency in the energy supply. Spectral index studies of NGC 326 will shed light on its history: the source has been observed at lower frequencies with the LOFAR LBA, and the new observations, together with complementary VLA and GMRT observations, will be used to study the spectral and other properties of the newly detected features in a forthcoming paper (Murgia et al. in prep.).

In the model we prefer NGC 326 becomes a member of the growing class of objects exhibiting this kind of complex interaction between the AGN-injected cosmic ray electrons and the cluster gas (see e.g. van Weeren et al. 2019 for a review). As in some of the best-studied cluster systems, there is no real boundary between plasma associated with the radio galaxy and material that is presumably moving with, and plausibly thoroughly mixed with, the intracluster medium; when the jets of NGC 326 switch off, the result will be a merging cluster with a population of distributed energetic cosmic rays and associated magnetic fields which may be re-energised by later shocks or compression to give rise to diffuse radio emission. Observations that allow the measurement of the spectral index or of polarization in the tail will help us to assess the extent to which it is now responding to the intracluster medium. There is little or no significantly detected polarization in an RM synthesis analysis of the LOFAR HBA data.

Observers inferring the presence of binary BH or BH-BH merger from X-shaped radio sources should be alert to the possibility of alternative, hydrodynamical explanations for the radio morphology and should ideally, before subscribing to a merger explanation, check that the wings in the sources of interest are sharply bounded in deep radio observations with good sensitivity to large angular scales. The LoTSS survey will allow the study of many more X-shaped sources in detail in the coming years.

ACKNOWLEDGMENTS

MJH and JHC acknowledge support from the UK Science and Technology Facilities Council ([ST/R000905/1], [ST/R00109X/1] and [ST/R000794/1]). HR and WLW acknowledge support from the ERC Advanced Investigator programme NewClusters 321271. RJvW acknowledges support of the VIDi research programme with project number 639.042.729, which is financed by the Netherlands Organisation for Scientific Research (NWO). We thank A. Shulevski, M.G.H. Krause, S. O’Sullivan, and E. Brinks for help-

ful comments on an earlier draft, and an anonymous referee for a constructive reading of the paper.

This research has made use of the University of Hertfordshire high-performance computing facility (<https://uhhpc.herts.ac.uk/>) and the LOFAR-UK compute facility, located at the University of Hertfordshire and supported by STFC [ST/P000096/1]. This research made use of ASTROPY, a community-developed core Python package for astronomy (Astropy Collaboration et al. 2013) hosted at <http://www.astropy.org/>, and of APLPY, an open-source plotting package for Python (Robitaille & Bressert 2012). This research has made use of the NASA/IPAC Extragalactic Database (NED), which is operated by the Jet Propulsion Laboratory, California Institute of Technology, under contract with the National Aeronautics and Space Administration.

LOFAR, the Low Frequency Array, designed and constructed by ASTRON, has facilities in several countries, which are owned by various parties (each with their own funding sources), and are collectively operated by the International LOFAR Telescope (ILT) foundation under a joint scientific policy. The ILT resources have benefited from the following recent major funding sources: CNRS-INSU, Observatoire de Paris and Université d’Orléans, France; BMBF, MIWF-NRW, MPG, Germany; Science Foundation Ireland (SFI), Department of Business, Enterprise and Innovation (DBEI), Ireland; NWO, The Netherlands; the Science and Technology Facilities Council, UK; Ministry of Science and Higher Education, Poland.

REFERENCES

- Amaro-Seoane P., et al., 2012, *Classical and Quantum Gravity*, **29**, 124016
 Astropy Collaboration et al., 2013, *A&A*, **558**, A33
 Begelman M. C., Blandford R. D., Rees M. J., 1980, *Nature*, **287**, 307
 Blandford R. D., Znajek R. L., 1977, *MNRAS*, **179**, 433
 Cava A., et al., 2009, *A&A*, **495**, 707
 Cheung C. C., 2007, *AJ*, **133**, 2097
 Cheung C. C., Healey S. E., Landt H., Verdoes Kleijn G., Jordán A., 2009, *ApJS*, **181**, 548
 Croston J. H., Ineson J., Hardcastle M. J., 2018, *MNRAS*, **476**, 1614
 Ebeling H., Edge A. C., Bohringer H., Allen S. W., Crawford C. S., Fabian A. C., Voges W., Huchra J. P., 1998, *MNRAS*, **301**, 881
 Ekers R. D., Fanti R., Lari C., Parma P., 1978, *Nature*, **276**, 588
 Fanaroff B. L., Riley J. M., 1974, *MNRAS*, **167**, 31P
 Gualandris A., Read J. I., Dehnen W., Bortolas E., 2017, *MNRAS*, **464**, 2301
 Hardcastle M. J., et al., 2016, *MNRAS*, **462**, 1910
 Hobbs G., et al., 2010, *Classical and Quantum Gravity*, **27**, 084013
 Hodges-Kluck E. J., Reynolds C. S., 2012, *ApJ*, **746**, 167
 Hodges-Kluck E. J., Reynolds C. S., Cheung C. C., Miller M. C., 2010, *ApJ*, **710**, 1205
 Krause M. G. H., et al., 2019, *MNRAS*, **482**, 240
 Laing R. A., Riley J. M., Longair M. S., 1983, *MNRAS*, **204**, 151
 Landt H., Cheung C. C., Healey S. E., 2010, *MNRAS*, **408**, 1103
 Leahy J. P., Williams A. G., 1984, *MNRAS*, **210**, 929
 Magorrian J., et al., 1998, *AJ*, **115**, 2285
 Merritt D., Ekers R. D., 2002, *Science*, **297**, 1310
 Murgia M., Parma P., de Ruiter H. R., Bondi M., Ekers R. D., Fanti R., Fomalont E. B., 2001, *A&A*, **380**, 102
 Offringa A. R., et al., 2014, *MNRAS*, **444**, 606
 Pilkington J. D. H., Scott J. F., 1965, *Memoirs of the Royal Astronomical Society*, **69**, 183
 Robitaille T., Bressert E., 2012, APLpy: Astronomical Plotting Library in Python, *Astrophysics Source Code Library* (ascl:1208.017)
 Shimwell T. W., et al., 2017, *A&A*, **598**, A104
 Shimwell T. W., et al., 2019, *A&A*, **622**, A1

- Slee O. B., 1995, *Australian Journal of Physics*, **48**, 143
- Smirnov O. M., Tasse C., 2015, *MNRAS*, **449**, 2668
- Tasse C., 2014, *A&A*, **566**, A127
- Tasse C., et al., 2018, *A&A*, **611**, A87
- Werner P. N., Worrall D. M., Birkinshaw M., 1999, *MNRAS*, **307**, 722
- Wirth A., Smarr L., Gallagher J. S., 1982, *AJ*, **87**, 401
- Worrall D. M., Birkinshaw M., Cameron R. A., 1995, *ApJ*, **449**, 93
- Wyithe J. S. B., Loeb A., 2003, *ApJ*, **590**, 691
- Zhang X.-G., Dultzin-Hacyan D., Wang T.-G., 2007, *MNRAS*, **377**, 1215
- Zier C., 2005, *MNRAS*, **364**, 583
- Zwicky F., Kowal C. T., 1968, "Catalogue of Galaxies and of Clusters of Galaxies", Volume VI
- van Haarlem M. P., et al., 2013, *A&A*, **556**, A2
- van Weeren R. J., de Gasperin F., Akamatsu H., Brügger M., Feretti L., Kang H., Stroe A., Zandanel F., 2019, *Space Sci. Rev.*, **215**, 16